



A Study on Booster Pump System with Flow Sensor for Individual Flow Control Method

M. Rakibuzzaman¹, H. H. Kim^{2†}, K. W. Kim³, S. H. Suh^{3†} and Y. S. Bae⁴

¹ Department of Mechanical Engineering, International University of Business Agriculture and Technology, Dhaka 1230, Bangladesh

² School of Mechanical Material Convergence Engineering, Gyeongsang National University, Jinju 52725, South Korea

³ School of Mechanical Engineering, Soongsil University, Seoul 06978, South Korea

⁴ Sego Industry Pump, Bongsu-daero, Seo-Gu, Incheon, Gyeonggi-do 22845, South Korea

†Corresponding Author Email: suhsh@ssu.ac.kr and khh106@gnu.ac.kr

(Received July 5, 2021; accepted December 14, 2021)

ABSTRACT

Booster pump system (BPS) can control the number of revolutions through an inverter by combining two or more vertical or horizontal centrifugal pumps in a series. Efficiency and energy savings, the most appealing aspects of booster pump systems, can be improved by controlling the operating conditions of individual pumps by measuring the flow rate of each pump. For improved operation, a booster pump system with a flow sensor to detect individual pump flow rates and a control algorithm to manage each low and high flow rate pump's revolutions per minute are critical. To achieve this, first, the turbine-type flow sensor was developed through computational fluid dynamics and experimentation. The flow sensor was improved using computational fluid dynamics, and its accuracy was validated through experiments. The resulting flow measurement accuracy of the designed flow sensor was within 4%, with a measurement uncertainty of 0.4%. In addition, an experimental pump facility was built and used to evaluate booster pump system performance to investigate the energy saving rate. Then, after driving one low-flow rate pump at a set pressure, the flow and frequency control operation algorithm was used. This algorithm increased the allowed output of the drive pump by increasing the inverter's frequency. When the frequency corresponding to the allowed output is achieved in the low-flow rate pump rather than the high flow rate pump, power savings increased due to the low-flow rate pump's extended drive range. The investigations on the developed system's energy consumption revealed that the energy savings were approximately 6.2% compared to the conventional system, depending on the system in question. The development of a booster pump system with a flow sensor was tested, and it was found to be effective.

Keywords: Booster pump; Flow sensor; Computational fluid dynamics; Experiment; Energy consumption.

NOMENCLATURE

| | | | |
|-----|------------------------------|---------------|--------------------------------|
| BPS | Booster Pump System | D | pipe diameter |
| CFD | Computational Fluid Dynamics | u | velocity |
| RPM | Revolution Per Minute | $S_{\bar{x}}$ | standard deviation of the mean |
| N | number of sample size | $U_{95\%}$ | measurement of uncertainty |
| Q | discharge flow rate | x_i | number of variables |
| S | standard deviation | | |
| T | time | | |

1. INTRODUCTION

In large-scale apartments and commercial buildings, rapid response to flow rate changes is required. A pump system controls the rotation speed through inverter by combining two or more vertical or

horizontal centrifugal pumps. Such a pump system is connected with various devices (pressure tank, pressure transmitter, suction/discharge conduit, control panel, and base) in series. Furthermore, a smart pump uses computer technology to judge and reason intelligent data independently and

effectively. The acronym SMART stands for self-monitoring, analysis, and reporting technology. In addition, BPS anticipates potential risks and communicates them to users via the host. The real-time monitoring of the pump operation status and automatic detection of abnormalities notifies the pump operators. To achieve this, the pumps of the same or different capacity are combined to operate under a fixed pressure. Further, to maximize energy savings, inverters are used to control each pump. If optimal energy savings are to be realized, the discharge flow rate of each pump in the BPS must be known. Besides, flow rate measurements for individual pumps can indicate abnormal statuses, such as idle, occlusion, and reverse flow. In contrast, conventional BPSs cannot detect failures or operation abnormalities in real time. The check valve installed in the discharge pipe or booster pump itself does not detect operational abnormalities in real time. Therefore, there is an urgent need to develop a method for detecting the booster pump's normal flow rate and malfunctions and dealing with them in real time (Chen 2000). In addition, the thermodynamic method is used to precisely measure the flow rate of each pump for a large capacity pump (ISO-5198, 1987; Bae *et al.* 2012a, 2012b). However, this method is difficult to apply due to the high cost and limited space of BPSs. Thus, a low-cost sensor system with high reliability is required for developing the BPS.

Several researchers have investigated pump optimization and flow characteristics numerically and experimentally. Zhou *et al.* (2019) examined the transient flow behavior near the reflux hole of the self-priming centrifugal pump numerically. The centrifugal pump was optimized by investigating the effect of addition of a splitter blade through numerical and experimental investigations (Namazizadeh *et al.* 2020). By using the design of experimental technique, the design space was created and the response surface method was used to obtain the optimum geometry; thus, increasing efficiency by 4.4%. Wu *et al.* (2020) combined CFD simulation with RBF neural network to optimize the performance of a mixed flow pump. Hence, they succeeded in increasing the pump's head and efficiency by 11.50% and 4.32%, respectively. Moreover, the effect of flow conditions on the instability of pump characteristics was analyzed numerically (Lipej 2021).

On the other hand, energy savings is the top priority for BPSs (Kaya *et al.* 2008); however, few studies have investigated energy savings in BPSs both experimentally and numerically (Carlson 2000; Schneider 2005; Ryu 1993; Lee *et al.* 2006; Armintor and Connors 1987). Saidur *et al.* (2012) studied the applications of variable speed drive (VSD) in electrical motors' energy savings. They showed that the application of VSD could improve the productivity while saving energy in pumps, fans, and compressors. Suh *et al.* (2015) presented a method for determining energy savings under variable speed conditions in a multistage, centrifugal pump. Unlike a constant speed pump system, the performance of a variable speed pump

cannot be evaluated using a fixed highest efficiency point. As an alternative, the energy savings compared to a constant speed pump system are calculated by measuring the power consumption according to the pump's operation pattern and comparing the constant speed and variable speed systems. Rakibuzzaman *et al.* (2015, 2017) investigated energy saving rates for a multistage, centrifugal pump with VSD, wherein input power values were obtained numerically and experimentally, resulting in a mean duty cycle derived from the flow patterns in the pump field. Besides, the hybrid model (Deng *et al.* 2018) for predicting discharge flow rate of reciprocating multistage pumps was investigated and formulated for practical application. In addition, the data-driven active learning methods (Deng *et al.* 2021) to actively explore informative data for smart modeling of dynamic multiphase flow processes have been applied to pump systems. Recently, an adaptive control method was used to estimate the real-time parameters of the centrifugal pump flow control systems (Wang *et al.* 2021). Furthermore, to maximize the energy savings of the variable speed operation pump system, accurate prediction of the operating point of each pump being operated is required. The pump's operating point is determined by the head and flow curves. However, current BPSs do not have the ability of directly measuring flow rate. Because the direct discharge flow rate is unknown, the operating point cannot be determined precisely. Thus, to find the optimum operating point, a method of predicting the pump's individual flow rates must be used through the discharge pressure of the pump and the amount of power of the motor. Nevertheless, in this case, it is impossible to accurately predict the number of switching points of the pump when constructing an optimized operating system to save power. To overcome this issue, a flow sensor can be installed in the check valve at the back of a single pump to measure its flow rate. When multiple pumps are operated at the same time, energy can be saved by operating a combination of the large and small capacity pumps until the operation of the multiple large capacity pumps is no longer required. Therefore, the link between BPS's energy saving effect and the flow sensor is significant.

This study aims to assess the flow measurement accuracy of each pump's flow sensor and develop energy saving technology based on flow sensor readings. A field test was used in this study to assess the flow measurement accuracy of a developed flow sensor. Further, computational approaches were used to solve the instability problem caused by installation position based on insertion depth. Energy consumption and energy saving technology using the flow sensor is also discussed in detail.

2. METHODOLOGY

2.1 Concept of Flow Sensor

Flow measurement depends upon the design of a flow sensor. Flow measurement accuracy is crucial

because various functions of the pump utilize the data from this sensor. A minimum distance of $10D$ to $20D$ from the measuring device is generally required in a flow rate measuring equipment (Besse *et al.* 2002; Bryant and Dennis 1996); however, insertion of a turbine-type flow meter into the check valve may result in flow instability because this minimum distance cannot be achieved. To mitigate this instability, experimental tests and numerical simulations were performed, leading to the modification of the shape of the check valve, followed by an error analysis (Angrisani *et al.* 2017; Arslan and Thomas 2002; Kim *et al.* 2017). There are several methods for measuring flow rate, but cost and space constraints of BPSs must be considered. Flow sensors are available in various types, including electromagnetic, turbine flow meter, ultrasonic flow meter, and magnetic Hall effect sensor.

The turbine flow meter for measuring the flow rate consisted of a rotating body, including a magnet element and a Hall sensor unit detecting the motion of the rotating body, as shown in Fig. 1. The rotating body comprises of five paddles, with each paddle containing a magnetic element inside. This rotating body generates five measurements per revolution, as shown in Fig. 1. The radius of the paddle was 8 mm, the length of the shaft was 15 mm, and the thickness of the paddle was 2.5 mm. Then, the flow rates were measured using a turbine-type flow meter with a magnetic Hall sensor.

The methodology adopted for measuring the flow rate using this flow sensor is as follows: the turbine flow meter rotates as fluid flows through the check valve (Chen 2000). The turbine flow meter is installed with a magnetic Hall sensor on the rotating paddles, as shown in Fig. 1. In the magnetic Hall sensor, current flows in a positive direction, which drives a magnetic field in the clockwise direction, generating varying voltage in the system (Kim *et al.* 2004; Urbański *et al.* 2015). The measured frequency of the flow sensor is passed on to the internally installed system, followed by conversion of this frequency to flow rate using various equations (Robinson *et al.* 1992).

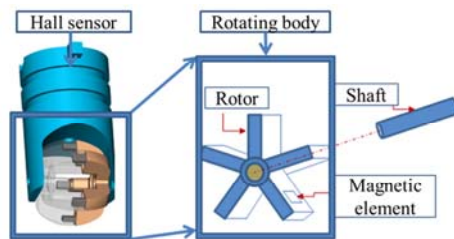


Fig. 1. Schematic of turbine flow meter.

The check valve with the built-in flow sensor is shown in Fig. 2. The developed flow sensor was installed in two model centrifugal pumps. The pump model SM510 was a small capacity pump,

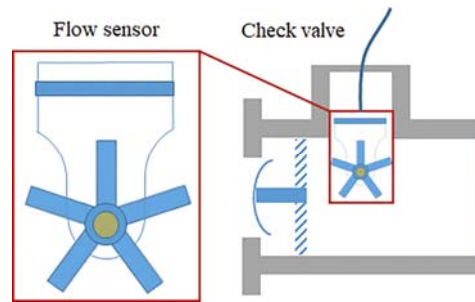


Fig. 2. Flow control check valve with a built-in flow sensor.

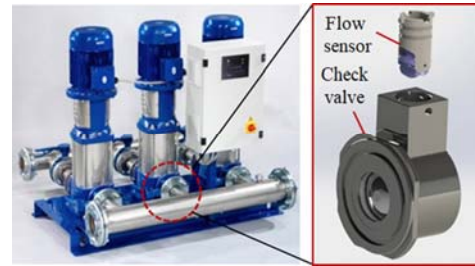


Fig. 3. Booster pump system with check valve (flow sensor inserted the check valve).

whereas SM1008 was a large capacity pump. To obtain flow sensor readings and determine measurement accuracy, three different pipes with diameters of 32, 40, and 50 mm were installed. The pump's rotational speed was 3430 revolutions per minute (RPM). The check valve was designed to accommodate various pipe diameters. In addition, the check valve was modified to facilitate the insertion of the flow sensor. The flow sensor can only fit into a narrow space in the check valve, and the chosen flow sensor was ideal for installation and removal in the modified configuration (Chen 2000; Robinson *et al.* 1992). When water flowed through the check valve in the BPS as shown in Fig. 3, the rotating flow sensor measured the frequency of each pump (Yogendra and Tadwakar 2014).

2.2 Flow Measurement Technology with Flow Sensor

2.2.1 Experimental Method

The test facility was constructed according to Korean Standard Association KS A-0515 guidelines (KS A 0515, 2006). Figure 4 presents the test layout and measuring test facilities of the BPS.

A centrifugal pump (4 kW) was installed in a reservoir tank of 0.7 m^3 , and a pressure gauge and electromagnetic flow meter were installed downstream of the pump. Pipe diameters from the check valve were 32, 40, and 50 mm, and the straight pipe section was installed at $5D$ intervals before and after the flow meter. A water temperature sensor was installed at the reservoir tank. To minimize vibration from the pump, the pump was fixed to the ground and the pipe around the check valve was fixed.

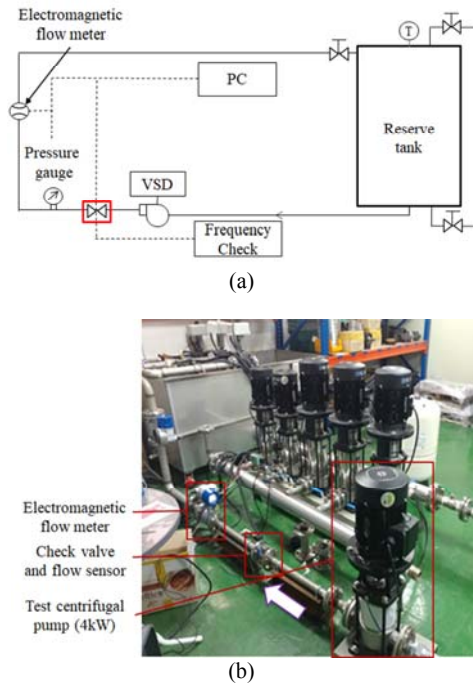


Fig. 4. (a) Experimental layout and (b) performance measuring test facilities of the pump system.

Downstream of the electromagnetic flow meter, a gate valve was installed to control flow rate and an inverter was installed to control the pump’s rotational speed. The system was connected to a computer (PC) to collect pressure, flow rate, and frequency of flow sensor readings. The preliminary test was conducted as follows: The reservoir tank’s water temperature was set to 20 °C. After stabilization, the pump was turned on, and the pressure and flow rates were measured. The variations in flow rate were used to control the gate valve. After changing the flow rate, the flow sensor’s frequencies were collected every second. Before proceeding to the next measuring point, the water temperature was recorded. After starting the pump, the flow rate was measured with an electromagnetic flow meter, and simultaneously the frequency of the flow rate sensor was measured, as shown in Fig. 5. The flow rate was modified by adjusting the gate valve at the end of the pipe. When the flow stabilized in the system, the flow rate and frequency were again measured, and the accuracy of flow rate measurement was evaluated. Next, the evaluated results were certified from the Korea Laboratory Accreditation Scheme guaranteed institute, which is a part of Korean Agency for Technology and Standards, Korea.

2.2.2 Error Analysis

Herein, the error in a measurement is defined as the difference between the measured value by a conventional flow meter and the measured value by a developed turbine-type flow meter. The term uncertainty quantifies the error that may have occurred around the measurement result. The uncertainty analysis is the process of estimating

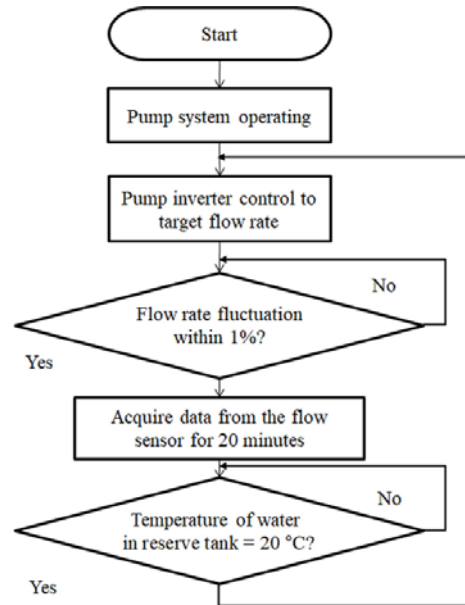


Fig. 5. Pump test procedure.

how great an effect the uncertainties in the individual measurements can have on the calculated result (Moffat 1988). In this experiment, the single-sample uncertainty analysis was chosen to measure the uncertainties. For this, consider a variable x_i with a known uncertainty S . The standard deviation of the population of measurements was taken to estimate the uncertainty interval, as described in Eq. (1) (Moffat 1988).

$$x_i = x_i(\text{measured}) \pm 2S, \quad (1)$$

where x_i is the true value, $x_i(\text{measured})$ is the measured value, and S is the standard deviation of the population from which the experimental observation was taken. The sample standard deviation S is expressed as Eq. (2) (Moffat 1988; Taylor 1982).

$$S = \left[\frac{1}{N-1} \sum_{i=1}^N (x_i - \bar{x})^2 \right]^{1/2}, \quad (2)$$

where $(x_i - \bar{x})$ is called the deviation of x_i and the factor N is the sample size. An uncertainty margin should lie within $\pm 2S$ of the mean which is 95% confidence level. At 95% confidence, it can be estimated the population mean must lie within $\pm 2S$ of the observation. Then error analysis was conducted using standard deviation of the means, standard error (SE) $S_{\bar{x}}$, an estimate of the population mean. The SE was estimated by the sample estimate of the standard deviation S (sample standard deviation) divided by the square root of the sample size N (Moffat 1988; Taylor 1982; JCGM GUM-6:2020):

$$S_{\bar{x}} = \frac{S}{\sqrt{N}} \quad (3)$$

The measurement of uncertainty U was calculated

using Eq. (4):

$$U_{95\%} = \left\{ \left(x_{i, fixed} \right)^2 + \left(2 \cdot S \right)^2 \right\}^{1/2} \quad (4)$$

where $x_{i, fixed}$ is the overall fixed error uncertainty of the measuring system (Moffat 1988). The final statement describing that x_i having an uncertainty is as follows: the estimate of x_i is the mean of $\bar{x}_i \pm$ the uncertainty interval $U_{95\%}$. In the experiment, uncertainty tests were conducted using a calibrated flow meter (Krohne OPTIMASS 6400C, Germany). Flow rates were varied from 40 to 200 L/min. The measurement device uncertainty was 0.4%, and the coverage factor was 2 at a 95% confidence level.

2.3 Energy Saving Method

2.3.1 Flow Detection Combination Method

Once the flow rate of each pump in the BPS is known, choosing the right operating protocol can reduce energy consumption over conventional operation methods. The variable speed operation control system has been used in conjunction with the large and small capacity pump control methods (Bae 2017). The developed combination product, i.e., the rotational-speed-adjusted small-large capacity pump, the nonrotational-speed-adjusted small-large capacity pump, and large capacity pump control methods, was investigated to test the performance of the variable speed pump system. The large capacity pump combination is used to configure the majority of BPSs in the large capacity pump control method. The large capacity pump control method sequentially increases the number of pumps used according to the required flow rate. The combination of small-large capacity pumps is used to maintain the required flow rate. Up to a maximum rotational speed of 60 Hz, switching from a small capacity pump to a large capacity

pump is possible. For the rotational speed-adjusted small-large capacity pump, power savings are compared to the large capacity pump using a small capacity pump. The flow sensor is installed in each pump to determine the point of operation from the large capacity to the small capacity pumps.

An algorithm demonstrating how the frequency control operation method with flow sensor helps to save energy is shown in Fig. 6. Energy saving rates were evaluated as a function of the mean duty cycle and input power of the system. Furthermore, the inverter can be used to control each pump to maximize energy savings; thus, making the necessary adjustments for optimal energy savings. First, the BPS checked the relationship between the out-pressure and set pressure. If the set pressure was higher than the out-pressure, the small pump would operate. When the required flow rate increased, RPM increased to meet the demand for a higher flow rate. The frequency was maintained by rechecking the out-pressure and set pressure. When the inverter frequency reached 60 Hz, the frequency was increased to 65 Hz, which varied the flow rate. While a conventional BPS would have switched to the large pump, the developed system continued to use the small pump, increasing its available frequency. Hence, the power consumption was reduced compared to the other pump combination methods.

2.3.2 Energy Usage Test Setup

A constant speed pump evaluates the performance of the pump in terms of efficiency. Certain information about the pump is required to measure its efficiency. Operating pressure, discharge flow rate, and input power are the parameters used to assess each pump's performance. However, because

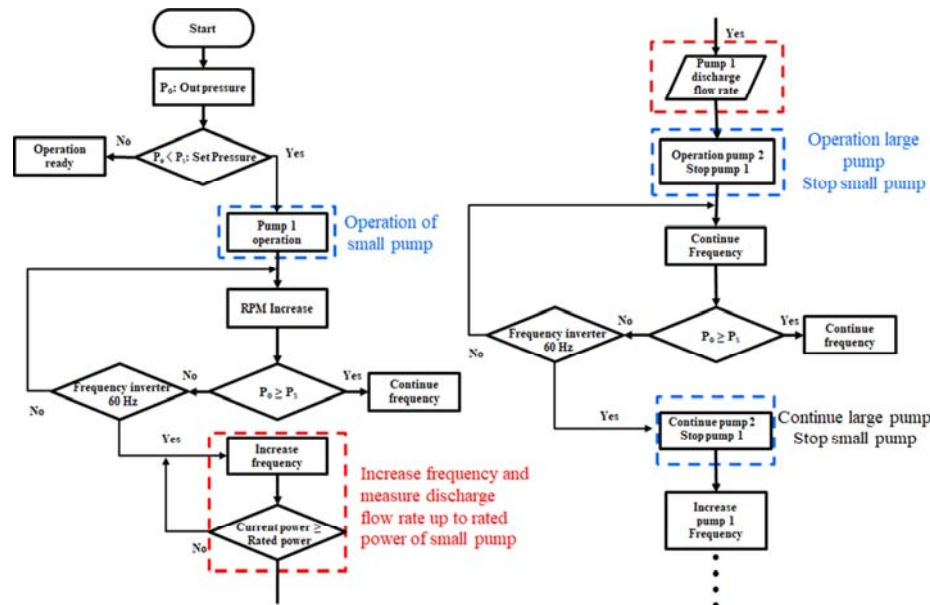


Fig. 6. Flow and frequency control operation algorithm (rotational speed-adjusted small-large pumps).

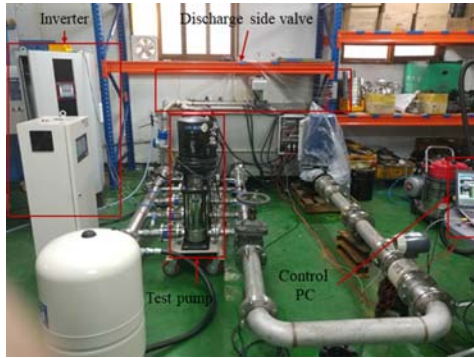


Fig. 7. Experimental pump facility for measuring energy usage.

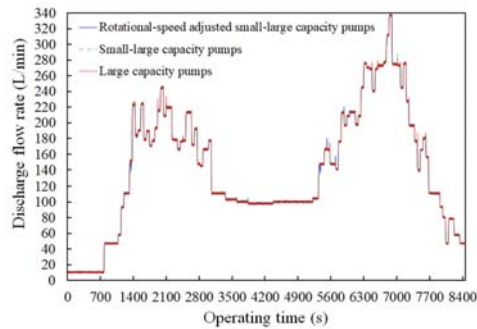


Fig. 8. Discharge flow vs. operating time.

Table 1 Check valve with flow sensor model grids.

| Grid description | Check valve | | Min. Y+ | Max. Y+ |
|------------------|-------------|---------|---------|---------|
| | Elements | Nodes | | |
| Coarse | 331,835 | 59,066 | 0.93 | 81.82 |
| Medium | 536,071 | 66,672 | 0.53 | 63.67 |
| Fine | 1,463,564 | 262,097 | 0.64 | 66.91 |

measurement of the discharge flow without a flow sensor is impossible, no device to measure the pump's efficiency is available for most BPSs. Instead, to estimate the pump's characteristics, the input power was obtained from the pump drive, and the individual load of the pump was measured. Thus, the overall efficiency of a conventional BPS can be calculated by dividing the hydraulic power by the input power ratio of the BPS. However, the BPS cannot maintain performance efficiency because it operates at a variable speed.

Following previous studies, energy usage was used to evaluate the performance of the BPS (Suh *et al.* 2014). Figure 7 depicts the experimental apparatus used for measuring BPS energy usage. A flow pattern describes the flow's behavior but in this work we used the term to refer to the flow consumption pattern. The flow consumption pattern was acquired and used to evaluate power consumption at the site, where the developed product was installed. Over one year, flow patterns were obtained from the apartment complex, where the development BPS was installed (Fig. 8). A representative flow pattern was obtained from the

measured flow patterns and used to analyze energy usage.

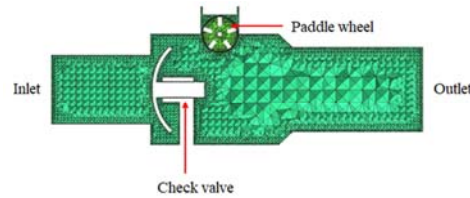


Fig. 9. Meshing grids of casing and impeller.

2.4 Computational Methodology

The design of a check valve and flow sensor was modeled by ANSYS ICEM (*Ansys Inc., Canonsburg, PA, USA, 16.2*). Unconstructed prism tetrahedral grids were created due to the complex internal geometry of the flow sensor system. The accuracy of the numerical analysis was increased by evaluating three types of grids: coarse-, medium-, and fine-meshed; and it was found that the medium-meshed grid yielded the best numerical accuracy (Kim *et al.* 2019; Rakibuzzaman *et al.* 2019). Total meshed elements and nodes were 536,071 and 66,672, respectively. Unconstructed meshing grids are shown in Fig. 9.

The quality of the grids is shown in Table 1. From the table, the 66,672 grid nodes showed the lower Y+ value compared to coarse and fine grid nodes. Therefore, the medium-meshed in Table 1 was chosen to simulate the check valve with flow sensor because it had the Y+ value within the required range for the prism-tetrahedral grids (Rakibuzzaman *et al.* 2019). The Y+ contour of the check valve is shown in Fig. 10.

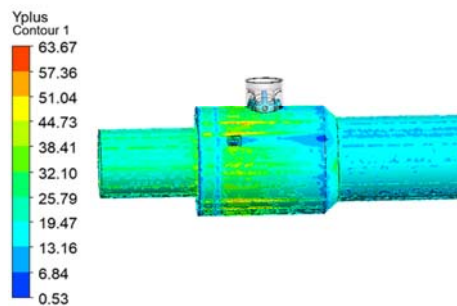


Fig. 10. Y+ contour of check valve with flow sensor.

A computational fluid dynamics (CFD) technique was applied to observe the internal flow field resulting from the flow measurement experiment using the ANSYS CFX 16.2 software. Numerical analysis of the flow was based on continuity and momentum equations (Eqs. (5) and (6), respectively) (Ansys Inc., 2016).

$$\frac{\partial u_i}{\partial x_i} = 0 \quad (5)$$

and

$$\rho \left(\frac{\partial u_i}{\partial t} + u_j \frac{\partial u_i}{\partial x_j} \right) = - \frac{\partial p}{\partial x_i} + \frac{\partial}{\partial x_j} \left(\mu \frac{\partial u_i}{\partial x_j} - \rho \overline{u_i' u_j'} \right) \quad (6)$$

where ρ and μ are density and dynamic viscosity, respectively, p is the pressure scalar, and $-\rho \overline{u_i' u_j'}$ is the apparent turbulent stress tensor. The k - ω -based shear stress transport (SST) model has been developed by [Menter \(1994\)](#) to effectively blend the robust and accurate formulation of the k - ω model in the near-wall region ([Ansys Inc., 2016](#); [Menter1994](#)). Moreover, the k - ω -based SST model provides highly accurate predictions of the onset and amount of flow separation under adverse pressure gradients ([Wilcox 1994](#)). In this model, the unknown turbulent viscosity μ_t was calculated by solving two additional transport equations for the turbulent energy k and turbulence frequency ω ([Wilcox 1994](#); [Georgiadis et al. 2006](#)). These two equations can be expressed as follows:

k equation:

$$\rho \frac{\partial k}{\partial t} + \rho u_j \frac{\partial k}{\partial x_j} = \frac{\partial}{\partial x_j} \left[\left(\mu + \frac{\mu_t}{\sigma_k} \right) \frac{\partial k}{\partial x_j} \right] + P_k - \beta' \rho k \omega + P_{kb} \quad (7)$$

and ω equation:

$$\rho \frac{\partial \omega}{\partial t} + \rho u_j \frac{\partial \omega}{\partial x_j} = \frac{\partial}{\partial x_j} \left[\left(\mu + \frac{\mu_t}{\sigma_\omega} \right) \frac{\partial \omega}{\partial x_j} \right] + \alpha \frac{\omega}{k} P_k - \beta \rho \omega^2 + P_{\omega b} \quad (8)$$

where P_{kb} is the shear production of turbulence. Here, σ_ω , σ_k , β , β' , and α are the model empirical values.

In comparison to the standard k - ϵ turbulence model, the prediction of flow detachment and the description of turbulence are much more accurate. As the SST model is based on both the k - ω and k - ϵ turbulence models, it produces accurate results both close to and far from walls ([Blazek 2001](#)). The model, on the other hand, is more complex; thus, requiring more computational time than simple two-equation models. Based on the experimental data, mass flow rate and relative pressure boundary conditions were imposed. All boundary walls were assumed smooth walls with no-slip conditions. The paddle wheel was rotating, and casing was in a stationary domain. At the rotating to stationary interface, a frozen rotor at a given rotational speed was chosen for steady-state analysis. To improve the accuracy of the numerical analysis, the convective term of the governing equation was discretized using a high-resolution scheme, and SIMPLE algorithms were used for solver control. The residual value of velocity and pressure was 1×10^{-5} and was controlled by convergence criteria. The simulation domain is presented in Fig. 11.

3. RESULTS AND DISCUSSION

3.1 Measurement of Flow Rate

Flow measurement results from the flow sensor were compared to those obtained from the

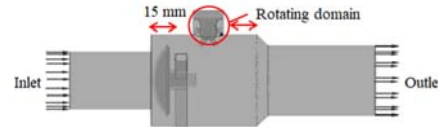
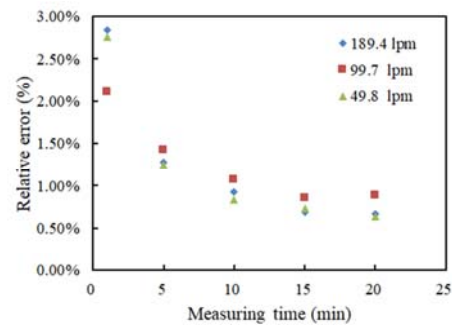
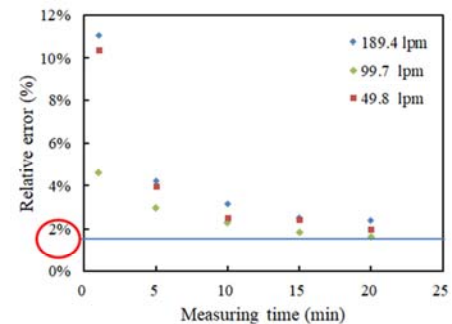


Fig. 11. Check valve with flow sensor domain for computer simulation.

electronic flow meter ([KS A 0515, 2006](#)), and the relative deviation between the electromagnetic flow meter and flow sensor was measured with varying time ([Seongwoo and Dennis 2006](#)). Figure 12 depicts the relative errors of the electromagnetic flow meter and flow sensor, and experiments showed that 15 min of measuring time was adequate. The SE for both the reference electromagnetic flow meter and the flow sensor was found to converge after 15 min. In this case, the flow sensor's measured relative errors were less than 2%. Table 2–4 shows the SE with measuring time only for 189.4, 99.7, and 49.8 L/min.



(a) Electromagnetic flow meter



(b) Flow sensor

Fig. 12. Relative error vs. measuring time of (a) electromagnetic flow meter and (b) flow sensor.

Although the measuring time was decided, the relationship between the electromagnetic flow and flow sensor remained unclear, particularly in the transient region. The other parameter was the flow sensor's inserted depth, which showed an unstable performance variation with depth. Figure 13 depicts a comparison of flow rate from the electromagnetic flow meter and frequency from the flow sensor. The flow rate range of the 50-mm

Table 2 Standard error with measuring time (189.4 *lpm*).

| Measuring time (min) | Flow rates (<i>lpm</i>) | Standard deviation of flow rate (<i>lpm</i>) | Standard error of flow rate (%) | Sensor output (Hz) | Standard deviation of sensor output (Hz) | Standard error of sensor output (%) |
|----------------------|---------------------------|--|---------------------------------|--------------------|--|-------------------------------------|
| 1 | 189.434 | 0.225 | 2.84 | 237.421 | 0.877 | 11 |
| 5 | 189.334 | 0.225 | 1.28 | 236.988 | 0.745 | 4 |
| 10 | 189.346 | 0.231 | 0.93 | 237.060 | 0.783 | 3 |
| 15 | 189.368 | 0.215 | 0.69 | 236.971 | 0.788 | 3 |
| 20 | 189.514 | 0.234 | 0.67 | 237.221 | 0.837 | 2 |

Table 3 Standard error with measuring time (99.7 *lpm*).

| Measuring time (min) | Flow rates (<i>lpm</i>) | Standard deviation of flow rate (<i>lpm</i>) | Standard error of flow rate (%) | Sensor output (Hz) | Standard deviation of sensor output (Hz) | Standard error of sensor output (%) |
|----------------------|---------------------------|--|---------------------------------|--------------------|--|-------------------------------------|
| 1 | 99.766 | 0.254 | 2.11 | 137.413 | 0.559 | 5 |
| 5 | 99.775 | 0.261 | 1.43 | 137.400 | 0.546 | 3 |
| 10 | 99.737 | 0.270 | 1.07 | 137.208 | 0.577 | 2 |
| 15 | 99.738 | 0.260 | 0.86 | 137.208 | 0.557 | 2 |
| 20 | 99.709 | 0.309 | 0.88 | 137.202 | 0.569 | 2 |

Table 4 Standard error with measuring time (49.8 *lpm*).

| Measuring time (min) | Flow rates (<i>lpm</i>) | Standard deviation of flow rate (<i>lpm</i>) | Standard error of flow rate (%) | Sensor output (Hz) | Standard deviation of sensor output (Hz) | Standard error of sensor output (%) |
|----------------------|---------------------------|--|---------------------------------|--------------------|--|-------------------------------------|
| 1 | 49.791 | 0.221 | 2.76 | 82.992 | 0.830 | 10 |
| 5 | 49.797 | 0.224 | 1.24 | 83.252 | 0.715 | 4 |
| 10 | 49.808 | 0.226 | 0.83 | 83.188 | 0.687 | 3 |
| 15 | 49.823 | 0.222 | 0.73 | 83.110 | 0.742 | 2 |
| 20 | 49.826 | 0.221 | 0.63 | 83.091 | 0.697 | 2 |

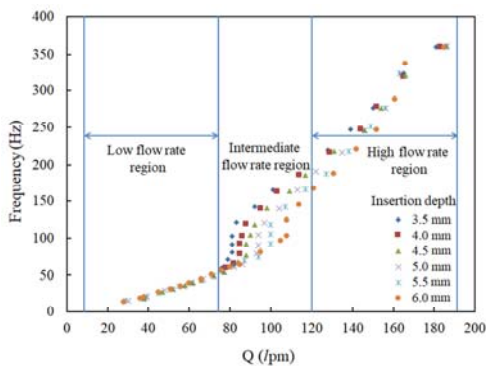


Fig. 13. Flow rate vs. frequency at varying flow sensor insertion depth.

Although there was a frequency difference depending on the insertion depth. For the 80–120 L/min, which is considered as a medium flow rate, the relationship between the flow rate and frequency was not proportional.

Based on the CFD results, the flow fields of the sensor and check valve were analyzed, resolving the nervous status, as shown in Fig. 14. Table 5 depicts the experimentally calculated relative deviations of different diameters. The flow sensor’s measurement

Table 5 Relative deviations of different diameters flow sensor.

| Dia. (mm) | Max. available flow rates (L/min) | Max. Deviation (%) | Min. Deviation (%) | Measurement of uncertainty (%) |
|-----------|-----------------------------------|--------------------|--------------------|--------------------------------|
| 32 | 200 | 0.84 | 0.23 | 0.37 |
| 40 | 300 | 3.98 | 1.48 | 0.40 |
| 50 | 600 | 1.70 | 0.52 | 0.40 |

accuracy was within a maximum of 4%, and measurement uncertainty was within 0.4%.

3.2 Energy Consumption

In this study, the energy consumption of the pump was also analyzed. The constant speed pump evaluates the superiority of pump performance in terms of efficiency (Asahara 1991). However, the BPS cannot show performance efficiency because it operates at variable speeds. It has been suggested to examine BPS performance using energy consumption (Kim *et al.* 2015), and energy savings from a variable speed centrifugal pump drive (Fox *et al.* 2012). To investigate energy consumption, we created three types of pumps in series (large capacity pump, small-large capacity pump, and

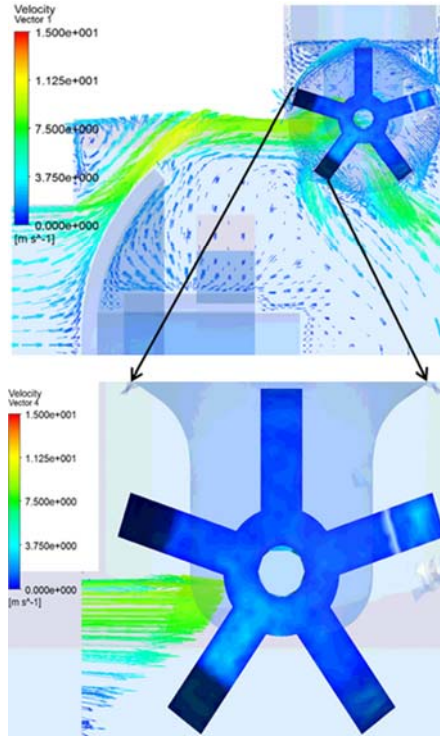


Fig. 14. Velocity distribution of check valve with flow sensor model.

rotational speed-adjusted small-large capacity pump). The site's flow pattern and BPS were used for performing the test (Taylor 1982; Seongwoo and Dennis 2006). Using the same flow rate pattern, the power consumption of the flow rate pumps in series, small-large pumps in series, and a newly developed system were compared. Figures 15 and 16 show the power consumption test and rate of power consumption results for the BPSs. The same flow pattern with power consumption was applied for 24 h to measure total energy consumption.

The energy consumption is calculated as input power (kW) × operating time (s) = input power consumption (kWh), as shown in Figure 15.

The energy saving rate for small-large capacity pump was calculated as input power consumption with small-large capacity pump/input power consumption with rotational speed adjusted small-large capacity pump. Furthermore, the energy saving rate for large capacity pump was calculated as input power consumption with large capacity pump/input power consumption with rotational speed adjusted small-large capacity pump.

The energy saving method increases the maximum driving frequency of the existing driving pump, which is currently set at 60 Hz, to an acceptable

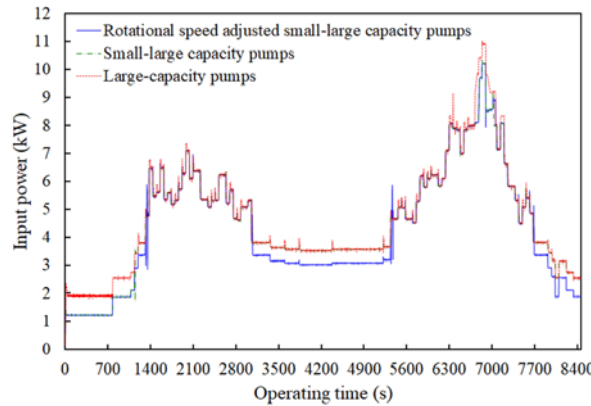


Fig. 15. Input power vs. operating time.

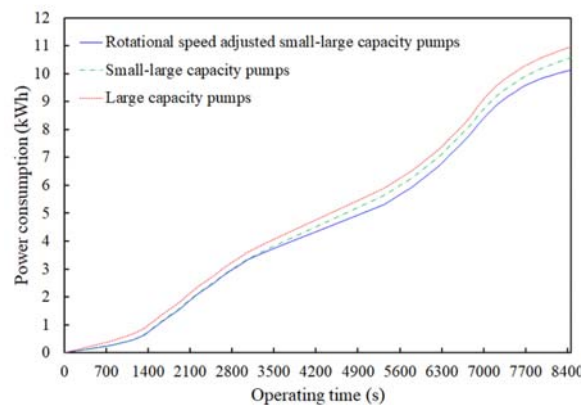


Fig. 16. Cumulative of power consumption.

Table 6 Power consumption according to pump operation method.

| Test list | Unit | Rotational-speed-adjusted small-large capacity pump | Small-large capacity pump | Large capacity pump |
|-----------------------------|------|---|---------------------------|---------------------|
| Power consumption | Wh | 100,569 | 106,018 | 106,853 |
| Relative error of pressure | % | - | 0.1 | 0.1 |
| Relative error of flow rate | % | - | 0.3 | 0.8 |
| Energy saving rate | % | - | 5.4 | 6.2 |

Table 7 Energy consumption of pumps.

| Description | Developed system | Large capacity pump | Small-large capacity pump |
|--------------------------|------------------|---------------------|---------------------------|
| Energy consumption (kWh) | 100.57 | 106.85 | 106.02 |

range of 65 Hz. The operating range at which the small and large capacity pumps have the same flow rates, discharge pressures can be expanded. Within the range of the operating point, small capacity pumps can save energy compared to large capacity pumps. When the system is applied, the energy saving rate may vary according to the usage pattern of the existing pump system.

The total energy consumption of the developed pump system was 5.4% compared to the small-large capacity pump and 6.2% compared to the large capacity pump, as shown in Tables 6 and 7.

4. CONCLUSION

To improve the energy savings of the BPS, a new pump combination and an appropriate operation method for the combination should be considered. The newly developed combination system, which is the rotational-speed-adjusted small-large capacity pump and nonrotational-speed-adjusted small-large capacity pump, and large capacity pump control method was investigated in the variable speed pump system.

The flow rate of each pump in the BPSs can be measured using the developed BPS that integrates various functions with a turbine-type flow meter using magnetic Hall effect. Experimentation and numerical simulations were performed to assess the accuracy of the developed flow meter and improve the stabilization of measurement to flow. To solve the problem of recurring instability, a computational approach was used. The flow measurement accuracy of the developed flow meter was evaluated. Experimental results revealed that the developed flow meter for the relation of flow rate to frequency had an error range of $\pm 5\%$.

The developed flow meter measures the flow rate of the small capacity pump and increases it to an acceptable frequency range through an inverter; thereby reducing energy consumption compared to using a large capacity pump.

Three types of combination systems (rotational-speed-adjusted small-large capacity pump, small-large capacity pump, and large capacity pump) were compared for power consumption using the same flow rate pattern.

When compared to other systems, the developed BPS's power consumption was reduced by

approximately 6%. A system that performs multiple functions was built by combining a BPS and flow meter. Flow measurement and frequency control were applied to the developed BPS, and this method improved the pump system's performance and reliability.

AUTHORS CONTRIBUTIONS

Md Rakibuzzaman conceived, analyzed the results, and wrote the paper; Hyoung-Ho Kim managed project administration, analyzed the results, and edited the draft; Kyungwuk Kim designed the flow sensor, conducted the experiments, and contributed in result analysis; Sang-Ho Suh contributed in fund collection and reviewed the entire work; and Young Seok Bae advised the project work. M. Rakibuzzaman and K. W. Kim contributed equally to this work.

ACKNOWLEDGMENTS

This work (Grant No. 201615081279) was supported by the Business for Cooperative R&D among the Industry, Academy, and Research Institute-funded, Korea Small and Medium Business Administration for the Promotion of Science.

CONFLICTS OF INTEREST

The authors declare no conflict of interest.

REFERENCES

- Angrisani, G., C. Roselli and M. Sasso (2017). Dehumidification and thermal behavior of desiccant wheels: correlations based on experimental and manufacturer data. *Heat Transfer Engineering* 39(3), 293–303.
- Ansys Inc. 2016, ANSYS-CFX (CFX Introduction, CFX Reference guide, CFX Tutorials, CFX-Pre User's Guide, CFX-Solver Manager User's Guide, Theory Guide), release 16.00, USA.
- Armintor, J. K. and D. P. Connors (1987). Pumping applications in the petroleum and chemical industries. *IEEE Transactions on Industry Applications* IA-23(1), 37–48.
- Arslan, S. and S. C. Thomas (2002). Grain yield

- mapping: Yield sensing, yield reconstruction, and errors. *Precision Agriculture* 3(2), 135–154.
- Asahara, T. (1991). Japan Association of Agriculture Engineering Enterprises, *Pumping Station Engineering Hand Book*. Tokyo, Japan.
- Bae, C., D. Vuong and H. Lee (2012a). A Study on the pump efficiency measurement using the thermodynamic method. *Journal of Korean Society of Marine Environment and Safety* 18(3), 267–272.
- Bae, C., D. Vuong and Y. Park (2012b, November). Pump efficiency instrumentation based on thermodynamic method and traditional technique. *Int. Conf. on Control, Automation and Information Sciences (ICCAIS)*, 359–363.
- Bae, Y. S. (2017, December). Flow sensor for booster pump and BPS real-time sensing malfunction. K. R. Patent No. 1018102320000.
- Besse, P. A., G. Boero, M. Demierre, V. Pott and R. Popovi (2002). Detection of a single magnetic microbead using a miniaturized silicon Hall sensor. *Applied Physics Letters* 80(22), 4199–4201.
- Blazek, J. (2001). *Computational Fluid Dynamics: Principles and Applications*. 1st Edition, Elsevier, United Kingdom.
- Bryant, J. A. and L. Dennis (1996, May). Effect of a 900 elbow on the accuracy of an insertion flow meter, results and comparisons for 4 and 6 in. diameter pvc pipe. *Proceedings of the Tenth Symposium on Improving Building Systems in Hot and Humid Climates*, Texas, USA 4(10), 48–59.
- Carlson, R. (2000). The correct method of calculating energy savings to justify adjustable-frequency drives on pumps. *IEEE Transactions on Industry Applications* 36(6), 1725–1733.
- Chen, Jerry S. J. (2000). On the design of a wide range mini-flow paddlewheel flow sensor. *Sensors and Actuators A: Physical* 87(1-2), 1–10.
- Deng, H., K. Yang, Y. Liu, S. Zhang and Y. Yao (2021, Aug.). Actively exploring informative data for smart modeling of industrial multiphase flow processes. *IEEE Transactions on Industrial Informatics* 17(12), 8357–8366.
- Deng, H., Y. Liu, P. Li and S. Zhang (2018). Hybrid model for discharge flow rate prediction of reciprocating multiphase pumps. *Advances in Engineering Software*.
- Fox, R. W., A. T. McDonald, P. J. Pritchard and J. C. Leylagain (2012). *Fluid Mechanics*. 8th edition, John Wiley and Sons, Inc., (Asia), New Jersey.
- Georgiadis, N. J., D. A. Yoder and W. B. Engblorn (2006). Evaluation of modified two-equation turbulence models for jet flow predictions. *AIAA Journal* 44(12), 3107–3114.
- JCGM GUM-6 (2020). Guide to the expression of uncertainty in measurement Part 6: Developing and using measurement models, Joint Committee for Guides in Metrology. Available on the web at <https://www.bipm.org/en/publications/guides/gum.html>
- ISO 5198 (1987) (E), Centrifugal, mixed flow and axial pumps-code for hydraulic performance tests-precision class, International Standard.
- Kaya, D., E. A. Yagmur, K. S. Yigit, F. C. Kilic, A. S. Eren and C. Celik (2008). Energy efficiency in pumps. *Energy Conversion and Management* 49, 1662–1673.
- Kim, H. H., M. Rakibuzzaman, K. Kim and S. H. Suh (2019). Flow and fast fourier transform analyses for tip clearance effect in an operating kaplan turbine. *Energies* 12, 264.
- Kim, K. W., S. H. Suh, H. H. Kim, M. Rakibuzzaman and Y. S. Bae (2017, 28 May -1 June), A study on a flow sensor connected with a check valve of a BPS, *10th international conference on computational heat, mass and momentum transfer*, Seoul, Korea.
- Kim, K. W., S. H. Suh and M. Rakibuzzaman (2015). Evaluation of energy savings for inverter driving centrifugal pump with duty cycles. *The KSFM Journal of Fluid Machinery* 18(6), 81–85.
- Kim, S. H., T. J. Nam and S. W. Park (2004). Measurement of flow direction and velocity using a micro machined flow sensor. *Sensors and Actuators A: Physical* 114(2-3), 312–318.
- KS A 0515 (2006). Method of flow measurement by turbine meters. Seoul, Korea, Korean Agency for Technology and Standards.
- Lee, J. H., K. H. Park and T. H. Hong (2006). Life cycle cost analysis of a general booster pump and high efficiency booster pump. *Journal of the Architectural Institute of Korea Planning & Design* 22(9), 259–266.
- Lipej, A. (2021). Flow conditions influence on the instability of a pump characteristic. *Journal of Applied Fluid Mechanics* 14(4), 1249–1255.
- Menter, F. R. (1994). Two-equation Eddy-Viscosity turbulence models for engineering applications. *AIAA Journal* 32(8), 1598–1605.
- Moffat, R. J. (1988). Describing the uncertainties in experimental results. *Experimental Thermal and Fluid Science* 1(1), 3–17.
- Namazizadeh, M., M. Talebian Gevari, M. Mojaddam and M. Vajdi. (2020). Optimization of the splitter blade configuration and geometry of a centrifugal pump impeller using design of experiment. *Journal of Applied Fluid Mechanics* 13(1), 89–101.
- Rakibuzzaman, M., H. H. Kim, K. Kim, S. H. Suh

- and K. Y. Kim (2019). Numerical study of sediment erosion analysis in Francis turbine. *Sustainability* 11, 1423.
- Rakibuzzaman, M., K. W. Kim, H. H. Kim and S. H. Suh (2017). Energy saving rates for a multistage centrifugal pump with variable speed drive. *Journal of Power Technologies* 97(2), 163–168.
- Rakibuzzaman, S. H. Suh, K. Kim, H. H. Kim, M. T. Cho and I. S. Yoon (2015). A study on multistage centrifugal pump performance characteristics for variable speed drive system. *Procedia Engineering* 105, 270–275.
- Robinson, J., J. Bryant, J. Haber and D. Turner (1992, May). Calibration of tangential paddlewheel insertion flow meters. *Proceedings of the Eighth Symposium on Improving Building Systems in Hot and Humid Climates*, Dallas, Texas, USA.
- Ryu, H. S. (1993). Water supply system using booster pumps. *Magazine of the SAREK* 22(1), 1–16.
- Saidur, R., S. Mekhilef, M. B. Ali, A. Safari and H. A. Mohammed (2012). Applications of variable speed drive (VSD) in electrical motors energy savings. *Renewable and Sustainable Energy Reviews* 16(1), 543–550.
- Schneider, B. (2005). Selection, operation and control of a work exchanger energy recovery system based on the Singapore project. *Desalination* 184(1), 197–210.
- Seongwoo, W. and L. Dennis (2006). The effect of elbows on the accuracy of liquid flow measurement with an insertion flow meter. *American Society of Heating, Refrigerating and Air-Conditioning Engineers* 112(1), 195–201.
- Suh, S. H., Rakibuzzaman, K. W. Kim, H. H. Kim, I. S. Yoon and M. T. Cho (2015). A study on energy saving rate for variable speed condition of multistage centrifugal pump. *Journal of Thermal Science* 24(6), 566–573.
- Suh, S. H., H. H. Kim, M. Rakibuzzaman, K. W. Kim and I. S. Yoon (2014). A study on the performance evaluation of variable-speed drive pump. *The KSFM Journal of Fluid Machinery* 17(5), 83–88.
- Taylor, J. R. (1982). *An introduction to error analysis*. 2nd Edition, University Science Books, Mill Valley, California, USA.
- Urbański, M., M. Nowicki, R. Szewczyk and W. Winiarski (2015). Flowmeter converter based on hall effect sensor. *Progress in Automation, Robotics and Measuring Techniques*, Springer International publishing, Cham, 352, 265–276.
- Wang, Y., H. Zhang, Z. Han, X. Ni (2021). Optimization design of centrifugal pump flow control system based on adaptive control. *Processes* 9, 1538.
- Wilcox, D. C. (1994). *Turbulence Modeling for CFD*. 1st edition, DCW Industries Inc., California, USA.
- Wu, X. F., X. Tian, M. G. Tan and H. L. Liu (2020). Multi-parameter optimization and analysis on performance of a mixed flow pump. *Journal of Applied Fluid Mechanics* 13(1), 199–209.
- Yogendra, P. J. and M. B. Tadwakar (2014). Implementation of GSM based water meter a step towards automation in billing system. *IOSR Journal of Electronics and Communication Engineering* 9(1), 1–4.
- Zhou, P., Z. Wu, J. Mou, D. Wu, S. Zheng and Y. Gu (2019). Effect of reflux hole on the transient flow characteristics of the self - priming sewage centrifugal pump. *Journal of Applied Fluid Mechanics* 12(3), 689–699.